PHILOSOPHICAL TRANSACTIONS OF THE ROYAL SOCIETY A MATHEMATICAL, PHYSICAL & ENGINEERING SCIENCES

Giotto Observations of Comet Halley Dust [and Discussion]

J. A. M. McDonnell, J. C. Zarnecki, R. E. Olearczyk, S. C. Chakaveh, G. S. A. Pankiewicz, S. T. Evans, Bernard Lovell, Fred Hoyle and S. Durrani

Phil. Trans. R. Soc. Lond. A 1987 **323**, 381-395
doi: 10.1098/rsta.1987.0093

Phil. Trans. R. Soc. Lond. A **323**, 381–395 (1987)
Printed in Great Britain

Giotto observations of Comet Halley dust

By J. A. M. McDonnell, J. C. Zarnecki, R. E. Olearczyk, S. C. Chakaveh, G. S. A. Pankiewicz and S. T. Evans

Unit for Space Sciences, University of Kent at Canterbury, Canterbury, Kent CT2 7NR, U.K.

Measurements of the dust environment of Comet P/Halley by the dust experiments on the *Giotto* and *Vega* spacecraft are discussed, as well as some aspects of the dust modelling that was carried out before the spacecraft encounters with the comet. These data have highlighted certain shortcomings in the models. For example, significant fluxes of grains ($m < 10^{-17}$ kg) smaller than allowed by the models have been detected, as well as a far higher ratio than predicted of light to dark side emission from the cometary nucleus. The mass-loss rate is determined and implications for the past history of the comet are discussed. It is also shown how the dust-impact data from the spacecraft experiments can be used to derive information on the distribution of emission over the surface of the nucleus.

1. Introduction

Within a period of eight days in March 1986, five spacecraft successfully achieved a close encounter with Comet Halley some five weeks after the comet's perihelion passage (on 9 February 1986). The closest approach to the cometary nucleus varied from *ca.* 7×10^6 km (for *Sakigake*) to *ca.* 605 km (for *Giotto*). A wide variety of scientific experiments was carried by these spacecraft involving dust, plasma and imaging instruments. Almost all experiments performed well and a vast quantity of data of unprecedented quality in terms of cometary research has been obtained. Very preliminary results have recently been presented (*Nature Suppl.* **321** pp. 259–366 (1986)).

2. *In-situ* dust measurements

The study of cometary dust was possible hitherto only through ground-based optical and infrared observations of the light scattered by the dust and of the thermal emission from the grains. This has led to some progress in the understanding of the nature of the grains but detailed understanding is possible only through *in-situ* measurements as carried out in particular by *Giotto* and *Vega* 1 and 2. Table 1 summarizes those experiments that made direct *in-situ* measurements of the dust. Other instruments provided further information on dust properties through remote sensing; e.g. on *Giotto*, the OPE (optical probe experiment) and HMC (Halley multicolour camera) measured the light scattered by the dust while the GRE (*Giotto* radio science experiment) measured the deceleration produced on the spacecraft by the impinging gas and dust; on *Vega* 1 and 2, the TVS (television system), IRS (infrared spectrometer) and TKS (three-channel spectrometer) instruments were all able to measure radiation scattered or emitted by the dust in various wavelength ranges (see table 2).

PHILOSOPHICAL TRANSACTIONS OF THE ROYAL SOCIETY A MATHEMATICAL, PHYSICAL & ENGINEERING SCIENCES

TABLE 1. SPACECRAFT EXPERIMENTS PERFORMING *IN-SITU* DUST MEASUREMENTS

spacecraft	instrument	instrument aims	principle of detection	limiting mass sensitivity/kg	geometric area/m^2	instrument mass/kg	coincidence detection
Vega 1 encounter, 6 March 1986 07h 20min 06s; miss distance, 8890 km; encounter velocity, 79.2 km s^{-1}	PUMA	dust particle elemental composition	time-of-flight ion mass spectrometer	3×10^{-19}	7.5×10^{-3}	19	coincidence with impact flash
	SP-1	dust particle flux and mass spectrum	impact plasma detection	10^{-19}	8.1×10^{-3}	2	internal? (positive and negative charge measurements)
	SP-2	dust particle flux and mass spectrum	piezoelectric and impact plasma detection	10^{-19}	5×10^{-2} (piezoelectric) 4×10^{-3} (plasma detection)	4	internal (three piezoelectric sensors)
							no
Vega 2 encounter, 9 March 1986 07h 20min 00s; miss distance, 8030 km; encounter velocity, 76.8 km s^{-1}	DUCMA	dust particle flux and mass spectrum	PVDF foil detection	1.5×10^{-16}	7.5×10^{-3}	3	no
	FOTON	large dust particle detection	foil perforation				
Giotto encounter, 14 March 1986; miss distance, 605 $\pm$ 8 km; encounter velocity, 68.4 km s^{-1}	PIA	dust particle elemental composition	time-of-flight ion mass spectrometer	3×10^{-19}	5×10^{-4} to 10^{-6} (dependent on impact rate)	9.89	coincidence with impact flash
	IPM-P	dust particle flux and mass spectrum	impact plasma detection	10^{-20}	1.19×10^{-2}	2.26 total	internal (positive and negative charge measurement) and possible coincidence with IPM-M
	IPM-M	dust particle flux and mass spectrum	piezoelectric detection	4×10^{-13}	1.19×10^{-2}		coincidence with IPM-P
	MSM	dust particle flux and mass spectrum	piezoelectric detection	4×10^{-12}	2.2		possibly internal (three piezoelectric sensors)
	RSM	dust particle flux and mass spectrum (front-shield penetration)	piezoelectric detection	10^{-9}	2.2		coincidence with front shield detectors
	CIS	dust particle counter	thin foil penetration	3×10^{-13}	0.1		possible coincidence with MSM

PHILOSOPHICAL TRANSACTIONS OF THE ROYAL SOCIETY A MATHEMATICAL, PHYSICAL & ENGINEERING SCIENCES

TABLE 2. CHARACTERISTICS OF ENCOUNTER: SPACECRAFT INSTRUMENTS PERFORMING REMOTE-SENSING OBSERVATIONS OF THE COMETARY DUST

spacecraft	instrument	type	dust-related aims	reference
Giotto	HMC	CCD telescope	imaging of dust jets and near-nucleus dust distribution through two narrow-band ($\Delta\lambda \sim 20$ nm) filters	Schmidt *et al.* (1986)
	OPE	photopolarimeter	determination of dust spatial density and scattering cross section by observing scattered light in three narrow-band filters ($\Delta\lambda \sim 3$–10 nm) and two polarizations	Levasseur-Regourd *et al.* (1986*a*)
	GRE	radio Doppler and ranging measurements	determination of total mass (dust and gas) impacting on spacecraft by observation of Doppler frequency shift due to atmospheric drag (no special on-board equipment required)	Edenhofer *et al.* (1986*a*)
Vega 1 and 2	TVS	CCD telescope	similar to *Giotto* HMC	Sagdeev *et al.* (1986)
	IKS	infrared spectrometer (2.5–5 μm and 6–12 μm), and imager (7–10 μm and 9–14 μm)	determination of dust spectral features and nuclear dust temperature	Combes *et al.* (1986)
	TKS	ultraviolet, visible and near infrared spectrometer	determination of dust spatial density and size spectrum from near-infrared scattered spectrum	Krasnopolsky *et al.* (1986)

2.1. *Measurements from the dust impact detection system, DIDSY*

The dust impact detection system (DIDSY) consists of five independent subsystems for the determination of the cometary dust efflux mass spectrum (figure 1) (McDonnell *et al.* 1986*a*). Three piezoelectric sensors mounted on the spacecraft-front dust-protection shield register dust grains of mass greater than 4×10^{-12} kg while a similar sensor mounted on the Kevlar rear shield detects the larger dust grains that can perforate the front shield ($m \gtrsim 10^{-9}$ kg). Mounted separately on the dust shield, the IPM (impact plasma and momentum) subsystem comprises a plasma detector (IPM-P) of limiting mass 10^{-20} kg, together with a piezoelectric crystal (IPM-M) fixed to the same target plate (limiting mass 4×10^{-13} kg). The IPM-P sensor consists of two identical halves, one of which is covered by a thin (*ca.* 2.5 μm) foil to provide limited particle density information. Also on the shield, the CIS (capacitor impact sensor), which comprises a thin film capacitor bonded onto the front shield, detects particles whose mass exceeds a threshold value of 3×10^{-13} kg. All these subsystems are controlled by the CDF (central data formatter), performing on-board data processing and formatting.

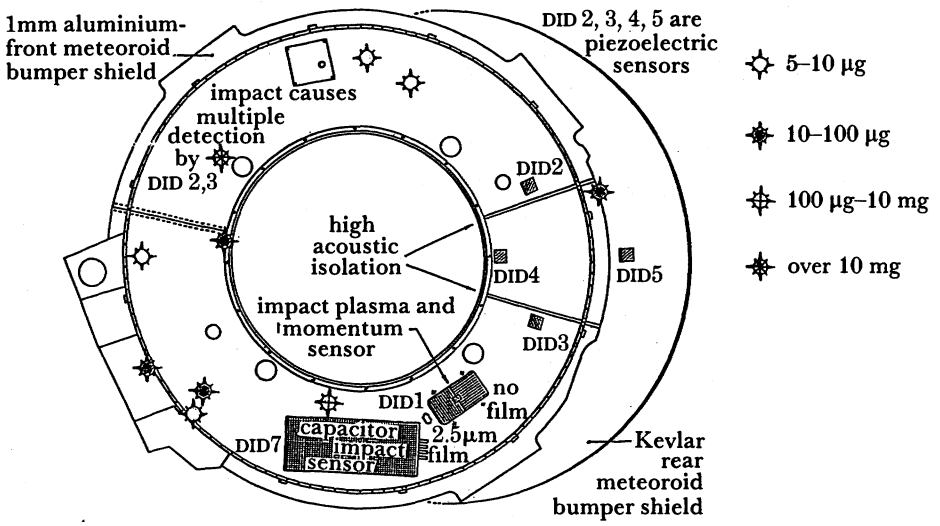

FIGURE 1. DIDSY sensor configuration on the outer dust shield and DID 5 on the rear Kevlar shield. Position of the ten largest particle impacts determined until now are indicated.

The properties of the subsystems and of the approximately 12000 impacts so far identified up to the point of encounter are summarized in table 3 (McDonnell *et al.* 1986*b*). All data in this table refer to the time period from first impact detection; up to −43 s for IPM-P, −5 s for MSM, RSM and IPM-M and −10 s for CIS. Time refers to encounter at 14 March 00h 11min 00s U.T. ground received time.

At −21 min an impact occurred on IPM causing saturation of both IPM-M and IPM-P giving a lower mass limit of some 5×10^{-11} kg. The CIS suffered a short circuit at −16 min which corrected itself at about −1 min. At approximately −44 s the largest mass, some 4×10^{-5} kg, was detected by all three front shield sensors. Around this time the IMP-P became erratic; the mode of operation of two of the MSM sensor (DID2 and DID3) became erratic and then changed to a fixed, non-preferred mode.

Preliminary analysis of the count rates from the various sensors has yielded fluxes of particles; a time profile shows the activity measured in the various mass ranges (figure 2).

PHILOSOPHICAL TRANSACTIONS OF THE ROYAL SOCIETY A MATHEMATICAL, PHYSICAL & ENGINEERING SCIENCES

TABLE 3. SUMMARY OF PERFORMANCE DATA AND MEASUREMENTS FROM DIDSY

sensor subsystem	limiting mass/kg	geometric area/m^2	effective area/m^2	first detection (time and distance)	total number detected†	peak rate/s^{-1}†	peak flux/$(m^{-2}\ s^{-1})$‡
DID 1 (IPM-M)	4×10^{-13}	1.19×10^{-2}	1.19×10^{-2}	−24 min (9.7×10^4 km)	1027	155 (−8 s)	4.5×10^4
DID 1 (IPM-PA) (sensor open)	10^{-20}	5.96×10^{-3}	5.96×10^{-3}	−62 min (2.5×10^5 km)	1100	31 (−49 and −44 s)	5.2×10^3
DID 1 (IPM-PB) (sensor+foil)	10^{-20} (+2.5 μm foil)	5.96×10^{-3}	5.96×10^{-3}	−36 min (1.5×10^5 km)	80	10 (−47 s)	1.6×10^3
DID 2/3 (MSM)	4×10^{-12}	1.94	2.5×10^{-1}§	−65 min (2.7×10^5 km)	1465	63 (−26 s)	1.5×10^3
DID 4 (MSM)	4×10^{-12}	2.2×10^{-1}	1.56×10^{-1}§	−70 min (2.9×10^5 km)	906	39 (−28 s)	5.2×10^2
DID 5 (RSM)	10^{-9}	2.2	~0.4 (est.)§	−208 s (1.4×10^4 km)	11	3 (−7 s)	7
DID 7 (CIS)	3×10^{-13}	10^{-1}	10^{-1}	−34 min (1.4×10^5 km)	7551	726 (−28 s)	5.3×10^4

† Not corrected for saturation and dead time effects.
‡ For all masses above the limiting mass.
§ Depends on incident mass spectrum (see text).

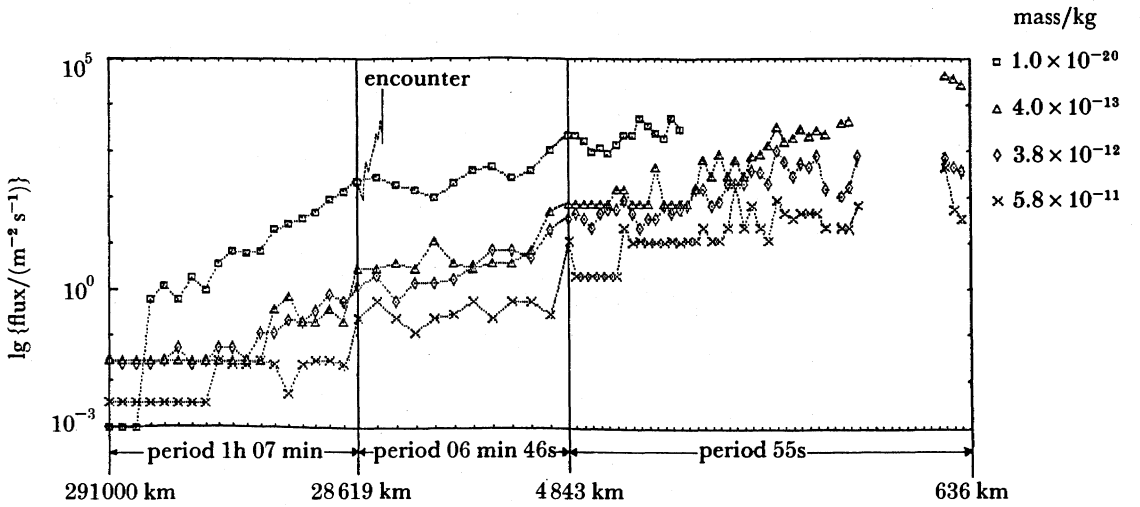

FIGURE 2. Flux rates (cumulative im mass) detected by various of the DIDSY subsystems, for the pre-encounter period, with the mass threshold limit for each profile shown. Note the expansions in the time axis for the rates nearest the time of closest approach. For comparison, the dotted line on the 1.0×10^{-20} kg line indicates, on the same timescale as the first period, the flux up to closest approach. No corrections are made for sensor dead-time effects, but this should be significant only for the last few seconds before closest approach.

3.1. *Cometary gas emission and dust acceleration*

The basis for the dynamical behaviour and distribution of dust is the so-called 'fountain model' based on Whipple's icy-nucleus model (Whipple 1950). This model can account for the motion of particles in the range 10^{-17}–10^{-3} kg; these are ejected with a velocity that depends on particle size, and move (relative to the comet nucleus) under the influence of radiation pressure (Divine 1981). The Halley encounters have shown many parameters assumed in the model to be ill-founded, but its general properties are substantiated.

The cometary nucleus is represented as a sphere of radius R_N of an inhomogeneous mixture of rocks, dust grains and volatile ices (Whipple 1950; 1951). The gas flux, related to the nucleus surface temperature T_N is given by (Delsemme & Swings 1952):

$$Z = P_s\,(2\pi \bar{M} k T_N)^{-\frac{1}{2}} \text{ kg m}^{-2}\text{ s}^{-1}, \tag{1}$$

where P_s is sublimation pressure, $\bar{M}$ is mean gas molecular mass, k is Boltzmann's constant and T_N is nucleus surface temperature.

This assumes that ice sublimes to form a gas with a molecular speed of

$$\bar{V} = (8kT_N/\pi\bar{M})^{\frac{1}{2}}. \tag{2}$$

Close to the nucleus surface, the sublimating ice–gas escapes with rate of Q_g kg s^{-1}, thereby accelerating the released dust; loading during expansion may be significant.

The radial flux of gas molecules at the surface of a spherical nucleus is given by

$$N = f(\zeta, \xi)\,(Q_g/R_N^2) \text{ kg m}^{-2}\text{ s}^{-1}, \tag{3}$$

where $f(\zeta, \xi)$ represents the source distribution function, and ζ and ξ are the spherical co-ordinates of the emission point on the surface of the nucleus (see §3.3).

Only dust grains that acquire enough force from the gas flow to overcome the nucleus's

gravitational attraction can escape from the comet and an upper limit of 3.3×10^{-3} kg is assumed now (Divine *et al.* 1986). The radial flux of such dust grains is described by a mass distribution $g(m)$ given by (Divine 1981)

$$\mathrm{d}N = \mu \bar{M} Q_g / R_N^2 f(\zeta, \xi)\, g(m)\, \mathrm{d}m \ \mathrm{m}^{-2}\ \mathrm{s}^{-1}, \tag{4}$$

where μ is the dust:gas mass ratio.

We have established a parametric form for the terminal velocity V_T of the liberated grains as a function of gas velocity V and particle radius, a, which encompasses the data of T. I. Gombosi (personal communication), namely

$$V_T = \bar{V} \frac{(a_g/a)^{\frac{1}{2}}}{1 + (a_g/a)^{\frac{1}{2}}}, \tag{5}$$

where $a_g = a_p\ (0.59/r_\odot)^{2.2}$ is the radius of the particle accelerated to $\frac{1}{2}V$ (which varies with heliocentric distance). For Halley near encounter we take

$$a_p = 2 \times 10^{-6}\ \mathrm{m},$$

$$r_\odot = \text{heliocentric distance in AU.}$$

Alternative and more complete forms have been given (see, for example, Delsemme & Miller 1971) but are less tractable in fitting observational data. Observational data from the Halley *Giotto* NMS instrument (Krankowsky *et al.* 1986) suggests a gas velocity of near 900 ms^{-1}, although pre-encounter modelling had assumed a value of *ca.* 660 ms^{-1}.

The motion of dust particles under radiation pressure results only in zero, one or two solutions at a point for dust trajectories from the nucleus, corresponding to locations beyond, on or within the envelope respectively. The 'two solution region' corresponds to trajectories originating directly from the nucleus or 'reflected' from the outer envelope. On the envelope these two solutions converge to produce an enhancement in local dust density.

A parameter η permits the specification of times of flight from the nucleus; the parameter is given by

$$\eta = \frac{R}{(2E+S) + [(2E+S)^2 - R^2)]^{\frac{1}{2}}}, \tag{6}$$

where R is the distance from the comet nucleus, S is the distance from the nucleus along the Sun–comet axis and E corresponds to the apex distance, which is the maximum distance any particle can travel in the sunward direction. The time of flight for travel from the nucleus for the two solutions is given by

$$t = (4ER\eta^{\pm 1})^{\frac{1}{2}}/V, \tag{7}$$

where η^{-1} and η^{+1} represent direct and reflected particles respectively. The ratio of the density of direct to reflected particles can be expressed as

$$\delta = \frac{f(\zeta_a, \xi_a)\, [(2E+S) + (2E+S)^2 - R^2]^{\frac{1}{2}}]}{f(\zeta_b, \xi_b)\, (R^2)}, \tag{8}$$

where $f(\zeta_a, \xi_a)$ and $f(\zeta_b, \xi_b)$ represent the source distribution functions for direct and reflected particles, respectively. Predicted values for *Giotto*'s trajectory show that δ varies from five at the edge of the outer envelope ($R = 10^5$ km) to 5×10^4 at the point of closest approach.

3.2. *Comparison with other models*

One shortcoming of the 'fountain model' is that it does not consider realistically the behaviour of large particles. As studied by Fertig *et al.* (1984), the larger particles have lower terminal velocities, which, because of the changing heliocentric distance, results in their confinement to a limited and asymmetric area around the nucleus–Sun line. This in turn causes the shape of the overall particle cloud to deviate greatly from the paraboloid of rotation typical of smaller particles.

In addition the 'fountain model' does not cater for the more general case where the nucleus moves around the Sun on a keplerian orbit. Models recently developed at ESOC (Massone *et al.* 1985) simulate such behaviour. The motion of dust particles in such cases can be expressed by

$$\boldsymbol{r} = \phi \boldsymbol{V} + \psi \Delta\kappa, \tag{9}$$

where $\boldsymbol{r}$ is the position vector of the dust particle, $\Delta\kappa$ represents the dependency of radiation pressure, $\boldsymbol{V}$ is the initial velocity vector of dust grains; and ϕ, ψ depend only on the orbit of the nucleus and the time of arrival at the required location.

It is essential to note that the pre-encounter mass distributions used to develop a framework for all modelling were determined explicitly from infrared observations of dust in comets. This was studied by several researchers such as Mukai (1977), Krishna Swamy & Donn (1979) and Hanner (1980).

Grain temperatures as a function of particle radius and heliocentric distance can be derived from theoretical modelling of thermal emission (Hanner 1982). These are obtained by equating the amount of solar energy absorbed by the grains to the thermal energy emitted by them. Because the emission is inefficient at wavelengths large compared with grain size, this relation shows that grains of a given temperature cannot radiate efficiently at wavelengths greater than ten times their radius and implies an observational limit for detection by infrared techniques of about 0.1 μm for the radius of emitting grains. Considering a typical density of about 1 g cm^{-3} for such particles, a mass cutoff of 10^{-16}–10^{-17} kg is implied. However, the data from *Giotto* and *Vega in-situ* dust experiments now demonstrate the existence of a high spatial density of grains with masses up to three magnitudes smaller than this limit (i.e. 10^{-20} kg) (McDonnell *et al.* 1986*b*).

3.3. *Nucleus emission model*

It is important to use a realistic function that describes the pattern of dust and gas emission from the nucleus. The Comet Halley Working Group uses the form (Divine 1981)

$$f(\zeta, \xi) = (0.0159)\ (5 - 3\cos\theta), \tag{10}$$

where θ is angular distance from antisubsolar point. The function has a maximum emission from the subsolar point and minimum from the antisubsolar point. This function accounts for emission due to both solar radiation and heating from the neighbouring coma and leads to a light–dark peak emission ratio of four. A new set of functions has now to be considered to account for the unexpected flux measurements from the spacecraft encounter with Halley.

PHILOSOPHICAL TRANSACTIONS OF THE ROYAL SOCIETY A MATHEMATICAL, PHYSICAL & ENGINEERING SCIENCES

Measurements show a strong concentration in forward ejecting jets, and hence a more concentrated function was tested, namely

$$f(\zeta, \xi) = (3/4\pi)\cos^2\theta,\ \theta > 90^\circ \quad \text{and} \quad f(\zeta, \xi) = 0 \quad \text{for} \quad \theta < 90^\circ. \tag{11}$$

Figure 3 shows the result of fitting to the cumulative mass obtained from DIDSY at a distance of 15600 km from the nucleus. The mass distribution, $g(m)$, and source function, $f(\zeta, \xi)$ of Divine (1981) have been used. The poor fit, as shown by discrepancies in the slope, flux and cut-off are indicative of the shortcomings inherent in much of the pre-encounter modelling. Better agreement between the *in-situ* data and theoretical models is being sought by using modified mass and source functions. It is already found that, for example, more concentrated source functions, of the type described above, do give an improved fit to the experimental data.

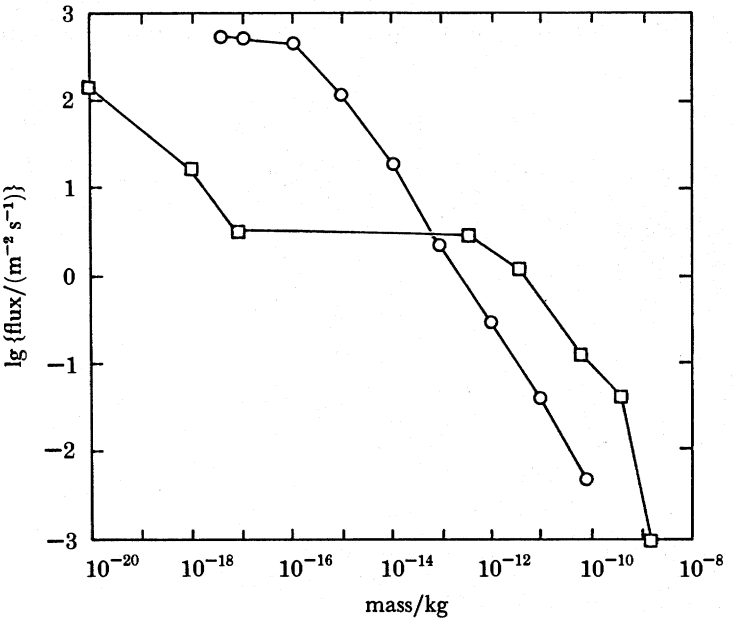

FIGURE 3. Comparison of actual and predicted cumulative mass spectrum at a distance of 15600 km from the nucleus. □, Measured DIDSY data over an integration period of 23 s; ○, predicted cumulative spectrum based on the dust model of Divine (1981). Discrepancies in slope, cut-off and flux level are clearly illustrated.

3.4. *Nucleus source activity mapping from direct fly-by measurements*

Recording the dust flux on the shield of *Giotto* has, of course, enabled the flux of particles to be measured along the spacecraft's trajectory. Because the typical apex distances of such particle trajectories are of the order of 10^5 km (Divine 1981), and the parabolae are approximately described by straight lines near the source, we can assume the dust particles to have travelled in a straight line between the emission point and the interception point at *Giotto*. In this way, the dust flux can be transformed back to a given position on the nucleus of the comet, according to the mass of particle arriving at the spacecraft, because the acceleration (occurring within several nuclear radii, namely *ca.* 15 km) is radial with respect to the comet nucleus (Divine *et al.* 1985).

Such a technique can be used to map active areas of the nucleus, where comparatively large

dust emissions have occurred. By making (θ_0, ϕ_0) the equatorial coordinates of the subsatellite point at closest approach, the subsatellite track can be drawn; a term resulting from the rotation of the nucleus is included to give the coordinates of dust emission θ_t, ϕ_t (see figure 4).

$$\begin{aligned}\theta_t &= \theta\ (\text{subsatellite}) + \theta\ (\text{emission point rotation})\\ &= \left\{-\arctan\left[\frac{V_s t \cos\epsilon}{R_0}\right] - \frac{t}{P_c}\times 360° + \theta_0\right\} - \left\{\frac{R}{V_T}\times\frac{360°}{P_c}\right\}, \qquad (12)\\ \phi_t &= \arcsin\frac{V_s t \sin\epsilon}{R} + \phi_0,\end{aligned}$$

where V_s is the spacecraft velocity, t is time after encounter, R_0 is the distance of closest approach, ϵ is the angle subtended by the nuclear equator and ecliptic along the trajectory, P_c is the rotation period, V_T is the terminal dust velocity and the subsatellite points are θ_0 and ϕ_0.

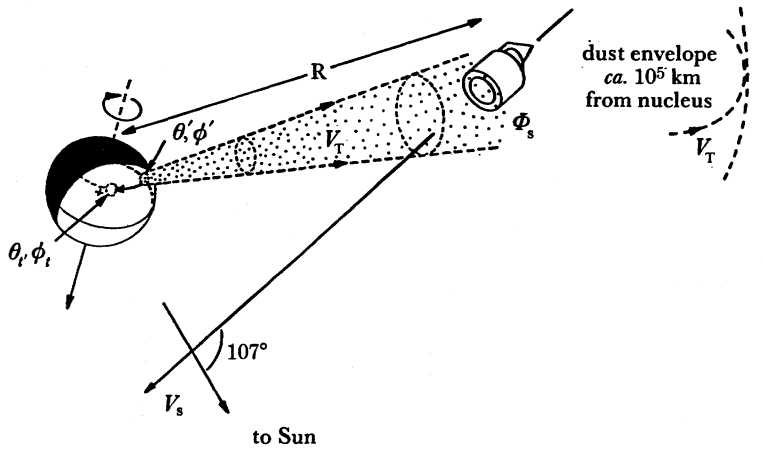

FIGURE 4. Encounter geometry near time of closest approach. Dust particles are emitted from point (θ', ϕ') and detected by *Giotto* at time t, by which time the emission point is situated at (θ_t, ϕ_t) relative to the spacecraft, due to nucleus rotation. $R_0 = 600$ km, $\theta_0 = 185°$, $\phi_0 = 25°$.

By looking at fluxes detected within different mass ranges, as distinct from threshold sensor measurements, whose terminal velocities are different, we have a dispersion of particle emission points around the nucleus. In this way, a picture of the nucleus can be built up by following back different particles to their appropriate emission points.

3.5. *Nucleus source mapping applied to* DIDSY *in-situ data*

A preliminary study of the potential for nucleus source mapping has been made with dust fluxes measured by the DID sensors. A total mass range is available from 10^{-20} kg to the maximum mass of 40 mg (largest particle); here, we show the tracks of emission points corresponding to $m_i = 10^{-11}$, 10^{-9} and 10^{-4} kg in figure 5. The subsatellite longitude and latitude of *Giotto* at closest approach are taken to be $\theta_0 = 185°$, $\phi_0 = 25°$ with $\epsilon = 58°$.

In figure 5 we also show the flux rate for the DID1M sensor, corresponding to particles of about 4×10^{-13} kg. This activity can then be related to the emission track of such masses (see §5). In this way, analysis of DIDSY data will reveal more detail of the nuclear surface.

PHILOSOPHICAL TRANSACTIONS OF THE ROYAL SOCIETY A MATHEMATICAL, PHYSICAL & ENGINEERING SCIENCES

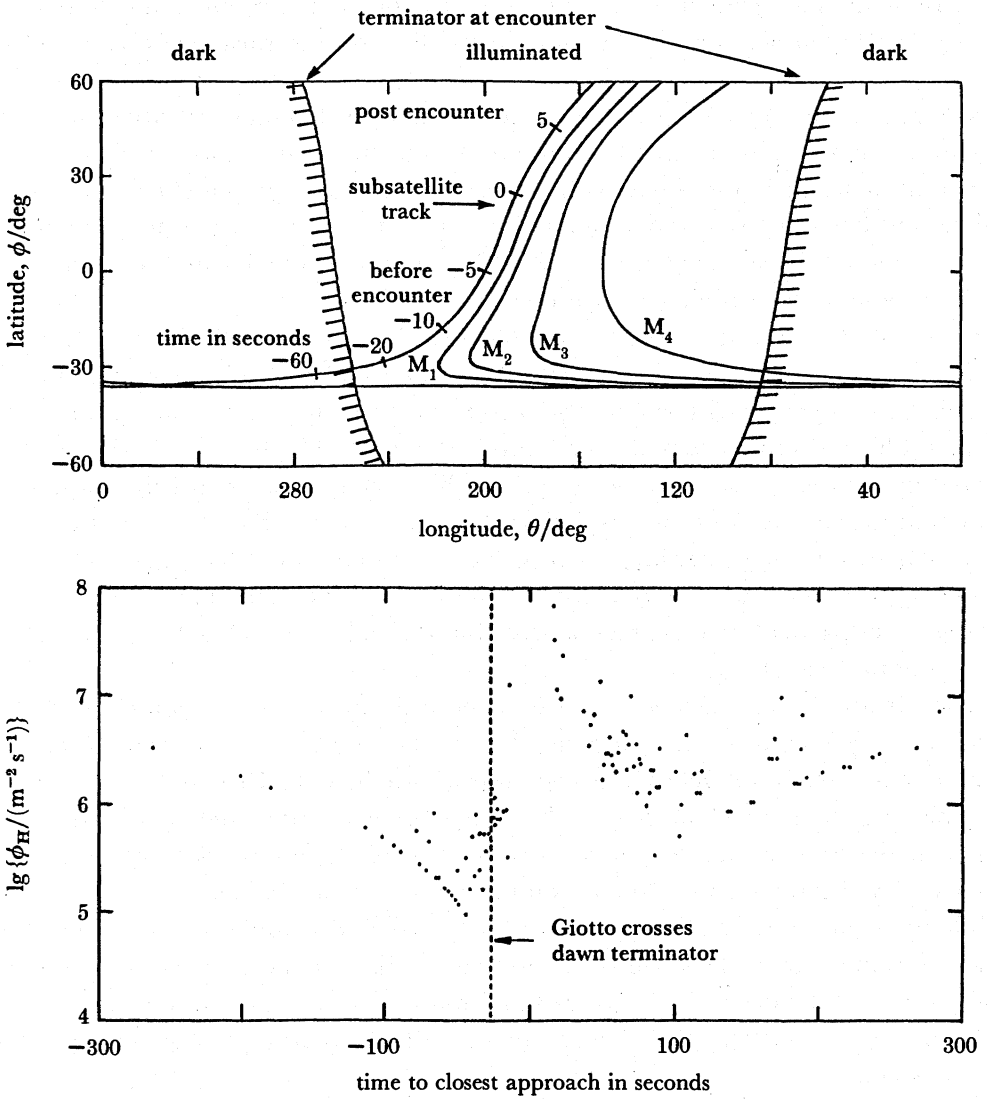

FIGURE 5. A latitude–longitude map showing emission tracks for particles of four different masses around Halley's nucleus. The track marked M_1 corresponds to masses of 4×10^{-13} kg, and a plot of the nucleus dust flux against time to closest approach is shown below. Tracks marked M_2, M_3 and M_4 correspond to masses of 10^{-10}, 10^{-8} and 10^{-6} kg, respectively. The subsatellite track is also shown, with tick marks indicating, in seconds, time to closest approach. We also show the flux at Halley, ϕ_H, normalized to an R^{-2} dependence for particles of mass 4×10^{-3} kg.

4. *Synergistic measurements related to* DIDSY

In addition to DIDSY, dust detection on the *Giotto* and *Vega* spacecraft is by the particulate impact analyser PIA and PUMA (Kissel 1986), which provides information on the composition of the individual dust particles and the average composition and mass distribution of cometary matter released by Halley. Preliminary results indicate the presence of H, C, N, O, Na, Mg, Si and Fe. One group significantly comprises particles that are rich in H, C, N and O. Contrary to expectations, carbonaceous chondrites fit only partially the mass spectra obtained for detected cometary particles. Furthermore, the spectra seem to indicate that the light elements specifically seem to have low mass to volume ratio, with particle densities perhaps as low as

0.01 g cm^{-3}. In general agreement with the results from DIDSY, PIA results indicate that small particles ($m < 10^{-17}$ g) are more abundant than implied by the dust models (Kissel *et al.* 1986).

The neutral mass spectrometer (NMS) determined the nature of Halley's volatile components, measuring the elemental and isotopic composition of the coma. As expected, water was the dominant parent molecule in the coma, with a density of 4.7×10^7 molecules cm^{-3} at 1000 km. The radial gas outflow velocity was determined to be 0.9 km s^{-1}, with a gas production rate of 6.9×10^{29} molecules s^{-1}. (Krankowsky *et al.* 1986). These data are of relevance to the *in-situ* dust data for the purpose of determining the dust:gas ratio.

The optical probe experiment (OPE) was able to measure the optical properties of the cometary dust by comparing the polarized spectral radiance observed at several points along the trajectory. Thus, together with results obtained from the Halley multicolour camera (HMC) (Keller *et al.* 1986) and ground-based observations (Green & Hughes 1987), the amount of light scattered by the dust or emitted by the gas can be directly measured. Initial results from OPE indicate that the emissivity of the dust follows an r^{-2} law for $r > 2000$ km from the nucleus, but increases at a greater rate closer in, probably due to sunward side enhancement (Levasseur-Regourd *et al.* 1986*b*) and with a flatter distribution at $r > 10000$ km. This is comparable in form with the DIDSY particulate cross section distribution and when related together the data will establish the particle albedo.

The cometary dust and gas fluence was also deduced from the deceleration of *Giotto* due to atmospheric drag by measuring the Doppler shift of the signals arriving from *Giotto* (radio science experiment). The total velocity change was approximately 16.7 cm s^{-1} implying that the total impacting mass on *Giotto* lies in the range 0.1–1 g (Edenhofer *et al.* 1986*b*), not conflicting with the DIDSY data. A detailed comparison of these data will follow now that extended telemetry records for the close encounter period are available.

By combining the results from all experiments, composition, distribution, mass and dynamics of the dust halo round the nucleus will be determined. This will allow the emission dynamics of dust and gas from the nucleus to be studied and more accurate assumptions to be made as to the genesis of comets, and the general accretion of matter into protoplanets in the prehistory of the Solar System.

5. Significance of encounter data

Although the data from the various spacecraft encounters are still at a very early stage of analysis, some broad conclusions can already be drawn from the data that refer specifically to the dust. Referring to the nucleus-mapping data, the first of which are presented in figure 5 for masses of around 4×10^{-13} kg, there appears to be a general increase in emitted flux as one proceeds further into the sunlit hemisphere of the nucleus. This may be indicative of a thermal-lag effect past the dawn terminator. From this data, we estimate the bright to dark side integrated flux ratio to be of the order of 20 to 30. As discussed earlier, existing models tend to adopt a smoothly varying source function of sinusoidal form. The function described by (10) predicts that this ratio is of the order of only 2. Additionally, camera images from *Giotto* and *Vega* show quite clearly that the emission is dominated by forward jet emission. Detailed analysis of the dust impact profiles will enable the relative importance of emission from the jets and the general background emission to be determined.

During the very close encounter period, we can use the DIDSY impact rates and derived mass

spectrum, combined with a $1/r^2$ model for the radial dependence of the dust distribution to determine the amount of dust in the line of sight from the spacecraft to the nucleus. For example, at a distance of 2000 km, we estimate that in a line-of-sight column to the nucleus, the integrated geometrical cross-sectional area of dust represents some 0.02 of the cross-sectional area of the column. This is consistent with the visibility of the nucleus as determined by HMC images (Keller *et al.* 1986).

Integration of the DIDSY flux rates yields a dust production rate of 3 t s^{-1}. Combined with data from NMS (Krankowsky *et al.* 1986), this gives a total mass rate of some 19 t s^{-1} at the time of *Giotto* encounter. Results from *Vega* 1 and 2 yield slightly different results, possibly indicative of variations in emission rates due to the dominance of jet activity. The *Giotto* results implies an erosion rate of some 0.5 m lost per perihelion passage. If we assume that Comet Halley was injected into the inner Solar System some 20000 years ago (Hughes 1985), this implies that the present mass is approximately half its original value. This mass-loss rate also suggests that the topology and current shape of the nucleus are dominated by ablation processes over the comet's lifetime in the inner Solar System, since the impact erosion rate on lunar rocks at 1 AU heliocentric distance is of the order of 1 mm Ma^{-1} (McDonnell & Ashworth 1972), i.e. corresponding to a negligible loss at each perihelion; evaporation is more than eight magnitudes more significant than impact erosion averaged over the orbit of Halley.

Several results of significance are suggested by preliminary analyses of the dust mass spectrometers (PIA on *Giotto* and PUMA on *Vega*). For example, one type of dust particle seems to be composed entirely of low-Z elements. Another type is only roughly similar to carbonaceous chondrites. Additionally some grains appear to have a low density. Also of considerable significance is that the dust observations of OPE, which yield the product of the dust local spatial density and the scattering cross section and the observations of DIDSY, when combined, will yield the grain albedo along *Giotto*'s trajectory.

From a technical viewpoint, the results from DIDSY have demonstrated the viability of the concept and design of the dual dust protection shield. This is potentially of great significance for future cometary missions. Results imply that approximately 1 % of the shield's surface area was ablated by dust impacts and that the total area penetrated by impacts was of the order of 1.5 cm^2.

Acknowledgements are due to all DIDSY coinvestigators and their collaborators, in particular those who supplied flight equipment or ground support hardware, namely W. M. Burton, E. Bussoletti, R. J. L. Grard, E. Grun, B. A. Lindblad, J.-C. Mandeville, R. F. Turner, J. G. Firth and G. C. Evans. The considerable efforts of the European Space Agency project team, the *Giotto* prime contractor, British Aerospace and cocontractors are also gratefully acknowledged. Financial support from the Science and Engineering Research Council to the Unit for Space Sciences, University of Kent is also acknowledged.

REFERENCES

Combes, M., Moroz, V. I., Crifo, J. F., Lamarre, J. M., Chara, J., Sanko, N. F., Soufflot, A., Bibring, J. P., Cazes, S., Coron, N., Crovisier, J., Emerich, C., Encrenaz, T., Gispert, R., Grigoryev, A. V., Guyot, G., Krasnopolsky, V. A., Nikolsky, Yu. V. & Rocard, F. 1986 *Nature, Lond.* **321**, 266.

Delsemme, A. H. & Swings, P. 1952 *Annls Astrophys.* **15**, 1.

Delsemme, A. H. & Miller, D. C. 1971 *Planet. Space Sci.* **19**, 1229.

PHILOSOPHICAL TRANSACTIONS OF THE ROYAL SOCIETY A MATHEMATICAL, PHYSICAL & ENGINEERING SCIENCES

Divine, N. 1981 ESA special publication no. SP-174, p. 25.
Divine, N., Fechtig, H., Gombosi, T. I., Hanner, M. S., Keller, H. U., Larson, S. M., Mendis, D. A., Newburn, Ray L. Jr, Reinhard, R., Sekanina, Z. & Yeomans, D. K. 1986 *Space Sci. Rev.* **43**, 1.
Edenhofer, P., Bird, M. K., Brenkle, J. P., Buschert, H., Esposito, P. B., Porsche, H. & Volland, H. 1986*a* ESA special publication no. SP-1077 p. 173.
Edenhofer, P., Bird, M. K., Brenkle, J. P., Buschert, H., Esposito, P. B., Porsche, H. & Volland, H. 1986*b* *Nature, Lond.* **321**, 355.
Fertig, J., Hechler, F. & Schwehm, G. H. 1984 *ESA bull.* **38**, 36.
Green, S. F. & Hughes, D. W. 1987 (In preparation.)
Hanner, M. S. 1980 In *The Solar System* (ed. I. Halliday & B. McIntosh),p. 223.
Hanner, M. S. 1982 In *Comets* (ed. L. Wilkening), p. 341. Tucson: University of Arizona Press.
Hughes, D. W. 1985 *Mon. Not. R. astr. Soc.* **213**, 103.
Keller, H. U., Arpigny, C., Barbieri, C., Bonnet, R. M., Cazes, S., Coradini, M., Cosmovici, C. B., Delamere, W. A., Huebner, W. F., Hughes, D. W., Jamar, C., Malaise, D., Reitsema, H. J., Schmidt, H. U., Schmidt, W. K. H., Seige, P., Whipple, F. L. & Wilhelm, K. 1986 *Nature, Lond.* **321**, 320.
Kissel, J. 1986 ESA special publication no. SP-1077, p. 67.
Kissel, J., Brownlee, D. E., Büchler, K., Clark, B. C., Fechtig, H., Grün, E., Hornung, K., Igenbergs, E. B., Jessberger, E. K., Krueger, F. R., Kuczera, H., McDonnell, J. A. M., Morfill, G. M., Rahe, J., Schwehm, G. H., Sekanina, Z., Utterback, N. G., Völk, H. J. & Zook, H. A. 1986 *Nature, Lond.* **321**, 336.
Krankowsky, D., Lämmerzahl, P., Herrwerth, I., Woweries, J., Eberhardt, P., Dolder, U., Herrmann, U., Schulte, W., Berthelier, J. J., Illiano, J. M., Hodges, R. R. & Hoffman, J. H. 1986 *Nature, Lond.* **321**, 326.
Krasnopolsky, V. A., Gogoshev, M., Moreels, G., Moroz, V. I., Krysko, A. A., Gogosheva, Ts., Palazov, K., Sargoichev, S., Clairemidi, J., Vincent, M., Bertaux, J. L., Blamont, J. E., Troshin, V. S. & Valníček, B. 1986 *Nature, Lond.* **321**, 269.
Krishna Swamy, K. S. & Donn, B. 1979 *Astron. J.* **84**, 697.
Levasseur-Regourd, A.-C., Bertaux, J. L., Dumont, R., Festou, M., Giese, R. H., Giovane, F., Lamy, P., Llebaria, A. & Weinberg, J. L. 1986*a* ESA special publication no. SP-1077, p. 187.
Levasseur-Regourd, A.-C., Bertaux, J. L., Dumont, R., Festou, M., Giese, R. H., Giovane, F., Lamy, P., Le Blanc, J. M., Llebaria, A. & Weinberg, J. L. 1986*b* *Nature, Lond.* **321**, 341.
Massone, L., Fertig, J., Grun, E., Schwehm, G. H. 1985 In *Asteroids, comets and meteors II* (Meeting at Uppsala University) (ed. C.-I. Lagerkvist, B. A. Lindblad, H. Lundstedt & H. Rickman), p. 407.
McDonnell, J. A. M. & Ashworth, D. G. 1972 *Adv. Space Res.* **13**, 333.
McDonnell, J. A. M., Alexander, W. M., Burton, W. M., Bussoletti, E., Clark, D. H., Evans, G. C., Evans, S. T., Firth, J. G., Grard, R. J. L., Grun, E., Hanner, M. S., Hughes, D. W., Igenbergs, E., Kuczera, H., Lindblad, B. A., Mandeville, J.-C., Minafra, A., Reading, D., Ridgeley, A., Schwehm, G. H., Stevenson, T. J., Sekanina, Z., Turner, R. F., Wallis, M. K. & Zarnecki, J. C. 1986*a* ESA special publication no. SP-1077, p. 85.
McDonnell, J. A. M., Alexander, W. M., Burton, W. M., Bussoletti, E., Clark, D. H., Grard, R. J. L., Grün, E., Hanner, M. S., Hughes, D. W., Igenbergs, E., Kuczera, H., Lindblad, B. A., Mandeville, J.-C., Minafra, A., Schwehm, G. H., Sekanina, Z., Wallis, M. K., Zarnecki, J. C., Chakaveh, S. C., Evans, G. C., Evans, S. T., Firth, J. G., Littler, A. N., Massone, L., Olearczyk, R. E., Pankiewicz, G. S., Stevenson, T. J. & Turner, R. F. 1986*b* *Nature, Lond.* **321**, 338.
Mukai, T. 1977 *Astron. Astrophys.* **61**, 69.
Sagdeev, R. Z., Szabó, F., Avanesov, G. A., Cruvellier, P., Szabó, L., Szegö, K., Abergel, A., Balazs, A., Barinov, I. V., Bertaux, J.-L., Blamont, J., Detaille, M., Demarelis, E., Dul'nev, G. N., Endroczy, G., Gardos, M., Kanyo, M., Kostenko, V. I., Krasnikov, V. A., Nguyen-Trong, T., Nyitrai, Z., Reny, I., Rusznyak, P., Shamis, V. A., Smith, B., Sukhanov, K. G., Szabó, F., Szalai, S., Tarnopolsky, V. I., Toth, I., Tsukanova, G., Valníček, B. I., Varhalmi, L., Zaiko, Yu K., Zatsepin, S. I., Ziman, Ya. L., Zsenei, M. & Zhukov, B. S. 1986 *Nature, Lond.* **321**, 262.
Schmidt, W. K. H., Keller, H. U., Wilhelm, K., Arpigny, C., Barbieri, C., Beirmann, L., Bonnet, R. M., Cazes, S., Cosmovici, C. B., Delamere, W. A., Huebner, W. F., Hughes, D. W., Jamar, C., Malaise, D., Reitsma, H., Seige, P. & Whipple, F. L. 1986 ESA special publication no. SP-1077, 149.
Whipple, F. L. 1950 *Astrophys. J.* **111**, 375.
Whipple, F. L. 1951 *Astrophys. J.* **113**, 464.

Discussion

SIR BERNARD LOVELL, F.R.S. (*Nuffield Radio Astronomy Laboratories, Cheshire, U.K.*). There are two meteor streams ascribed to Comet Halley as a source. How do your data relate to these streams?

PHILOSOPHICAL TRANSACTIONS OF THE ROYAL SOCIETY A MATHEMATICAL, PHYSICAL & ENGINEERING SCIENCES

J. A. M. McDonnell. From the *Giotto* DIDSY data we have established two input parameters that would assist in this correlation, namely (i) the size spectrum or mass index and (ii) the total mass input potentially available for such streams generated by Comet Halley during its 1986 perihelion passage. The latter is, of course, determined only up to a limiting sensitivity corresponding to some 40 mg, but certainly corresponds to a second-magnitude photographic meteor or brighter. The mass index of the dust distribution may well differ from that observed in the streams because of observational factors and evolutionary changes within the perhaps 20000 year old particles in the stream.

Sir Fred Hoyle, F.R.S. (*Department of Applied Mathematics and Astronomy, University College, Cardiff, U.K.*). In passing from particle masses to their densities, volumes are needed. How were the volumes obtained? Were they from areas, taken to be $(\text{area})^{\frac{3}{2}}$?

J. A. M. McDonnell. Particle density is deduced by the particle impact analyser (PIA) (principal investigator Dr J. Kissel, Heidelberg) by consideration of the ionization from incident particles compared with the impact ionization which that particle causes from the silver target material. Such a ratio is a measure of the average mass per unit area of the particles, derived by their effective penetration into the PIA silver target. Interpretation is tentative as yet (not published).

S. Durrani (*Department of Physics, University of Birmingham, U.K.*). Is there any information on the material strength or density of the particles impacting the *Giotto* spacecraft from the DIDSY experiment?

J. A. M. McDonnell. At the *Giotto* impact speed of 68 km s^{-1}, the particle strength has a very minor effect on penetration ability and therefore inferring particle density from the DIDSY data is not straightforward, especially for particles penetrating the shield. For one range of masses, however, the high-sensitivity DIDSY IPM-P sensor has two separate parts, identical except for a 2.5 μm foil covering one part. From comparison of these with the subunits, the penetration limit may be obtained but such data are still under analysis.

Note added in proof (30 *May* 1987). In the more recent analysis of the data from DIDSY and PIA the database has been extended and instrumental calibration factors reassessed. It is now seen that the flux of the smaller particles on the IPM-M and P sensors before encounter was suppressed because of the malfunction of a thin protective Mylar cover (22 μm); this was indeed abraded totally at 10 s before encounter but does explain some of the anomalies characteristic of the pre-encounter DIDSY mass distribution (figure 3) where fluxes plotted at masses 10^{-20}, 10^{-18} and 10^{-17} kg are now seen to correspond to residues from larger penetrating particles in the mass range 10^{-15} to 10^{-12} kg. Revised and extended data are published in J. A. M. McDonnell *et al.* ESA Special Publication SP250 (1986).

PHILOSOPHICAL TRANSACTIONS OF THE ROYAL SOCIETY A MATHEMATICAL, PHYSICAL & ENGINEERING SCIENCES